Image Color Balance with Laplacian and Gaussian Pyramid (CBLGP) Algorithm

Hojiwala Robin[a], Vijay Patil[b], Jayshri Patil[c],Vinay Pathak[d]

[a]*P P Savani University, Kosamba, Surat and 394125, India*
[b]*P P Savani University, Kosamba, Surat and 394125, India*
[c]*P P Savani University, Kosamba, Surat and 394125, India*
[d]*P P Savani University, Kosamba, Surat and 394125, India*

Abstract

In recent times, technology has rapidly and significantly evolved across all sectors. Digital image processing stands out as a modern technology aimed at achieving clear images. However, digitized images often encounter issues of low quality, such as unclear or underwater images that require enhancement for better visibility. These problems stem from factors like deficient focusing, lighting, and various constraints leading to low contrast, shading, and artifacts. Underwater and satellite images consistently face less-than-ideal conditions due to environmental factors like light refraction in water, particle scattering, and dust in aquatic environments. Similarly, challenges in space, such as poor illumination and lack of contrast, further complicate image analysis. Overcoming these obstacles is crucial for extracting valuable information, necessitating advanced processing techniques. This paper introduces an enhanced Gaussian/Laplace color balance-fusion algorithm designed to improve image visibility. Modifications to certain equations result in sharper and clearer images. The algorithm begins by determining the white balance of the input RGB color image and subsequently enhances its intensity. Edge improvement is carried out separately using a depth filter. The weights for each image are then determined and combined to form a Laplace Pyramid. A color restoration technique is applied to process the resulting image, producing the final enhanced image. While existing methods for image contrast enhancement typically focus on image features, they often neglect user characteristics. This paper explores the application of image sharpening, a prominent image enhancement technique, in clearing underwater or low-quality images using the proposed algorithm.

Keywords: EDSHE, High pass filter, White patch ratix, Laplacian pyramid, Color restoration.

1. Introduction

In the contemporary era, images are sourced from diverse environments such as space, underwater, and landscapes, yet a common challenge persists—blurry or unclear images. Recently, experts have increasingly focused on addressing the unique difficulties of enhancing underwater images, recognizing their significance in scientific studies. The quality of images is vital not only for scientific research but also in medical image analysis, where understanding the intricacies of different body parts is essential.

Similarly, in underwater scientific activities, addressing blurry images is crucial for studying water conditions and identifying organisms.

Dealing with blurry images in real-world scenarios involves necessary steps like enhancing and sharpening, managing brightness and contrast, removing noise, and sharpening edges. Comprehensive image enhancement also requires color correction.

In various sectors, image analysis plays a crucial role, aiding in disease diagnosis in the medical field, identifying weather patterns through satellite images, monitoring the environment, ensuring security through enhanced surveillance images, and enhancing the understanding of astronomical phenomena.

Digital image processing, applicable across diverse fields, faces challenges due to algorithms requiring human intervention and being computationally complex. To address these challenges, a popular recent approach involves dehazing based on visible and near-infrared (NIR) image combinations. Digital camera sensors can capture both spectra simultaneously, and modifying filters allows for capturing either visible or NIR images. Dehazing with NIR images proves effective due to their high contrast and ability to see through haze, providing bright responses for flora & fauna and atmosphere around us. Researchers use pairs of visible–Near Infrared (NIR) images to estimate air light and transmission, and alternative algorithms without air light estimation have also been proposed in literature [20, 21, 22, 23, 24, 25]. For a comprehensive understanding of NIR image acquisition, detailed resources and documentation are recommended.

The algorithm employs diverse image types and is applied to a range of images to enhance results, particularly in the case of blurry images. Through its demonstration, the algorithm underscores the potential for developing a more reliable approach, given the drawbacks associated with existing methods. Consequently, this study introduces a refined version of an already-established algorithm. This enhanced iteration incorporates superior procedures for brightness and contrast enhancement, implements an improved sharpening technique, and integrates a color restoration process. These augmentations collectively elevate the proposed algorithm, surpassing both its original version and other existing algorithms.

2. Proposed algorithm

The primary objective of the proposed algorithm is to extract high-quality images with enhanced details and color information from their blurred counterparts. In this literature review, the algorithm's role is emphasized in improving images.

The algorithm operates in a sequential manner: it begins by taking in the input image. Subsequently, a white balancing process is initiated, combining the White Patch Retinex and the Gray World Assumption algorithms for rectify image color distortions. Following this step, two images are generated. The first undergoes brightness and contrast enhancement through the AEIHE (Adaptive Entropy Index Histogram Equalization) algorithm, while the second is subjected to sharpening using unsharp masking with a high-pass filter to accentuate acutance details.

Next, weighting maps are determined for fusion. The algorithm employs Laplacian and Gaussian Pyramid fusion techniques to enhance the image. The resultant output image exhibits improved color and enhanced acutance. "Figure 1" illustrates the diagram of the Color Balance with Laplacian and Gaussian Pyramid (CBLGP) algorithm.

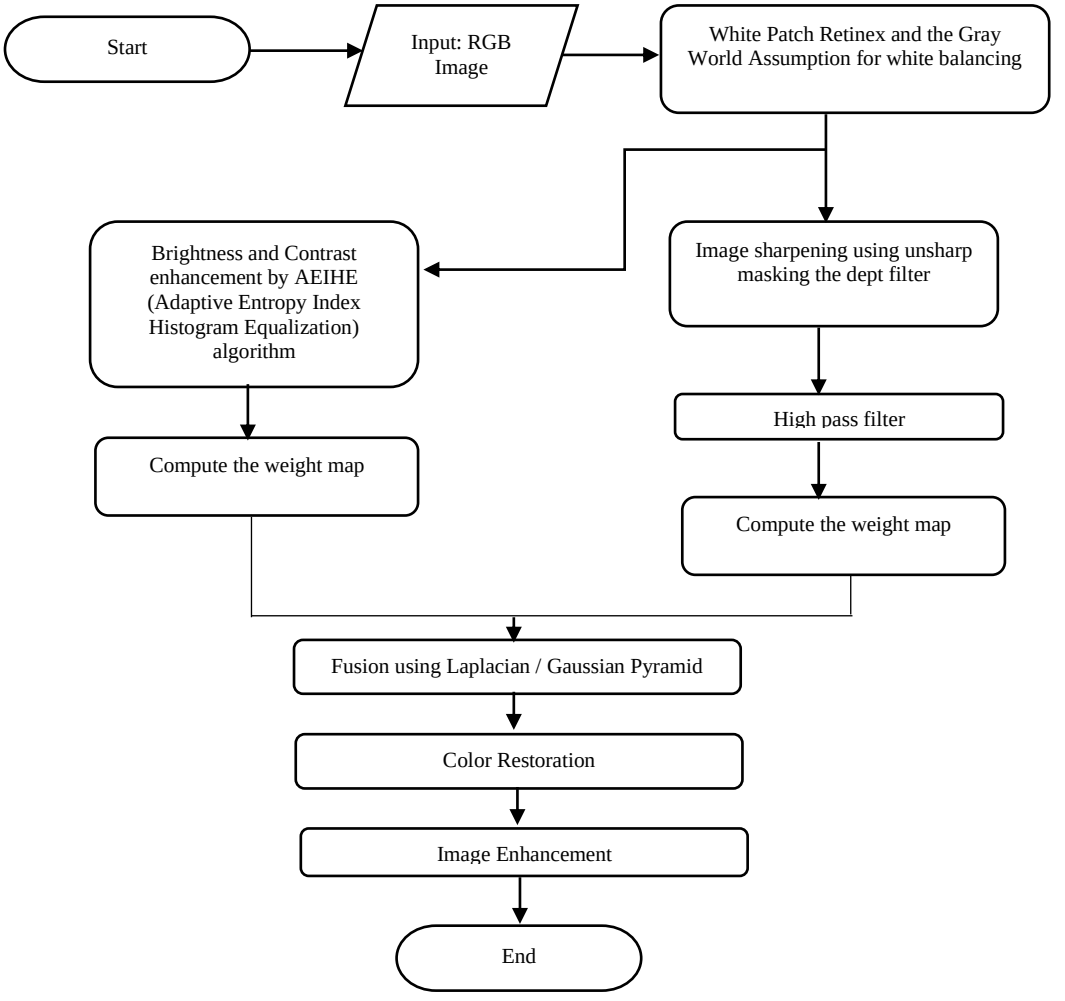

Fig 1: Color balance with Laplacian and Gaussian Pyramid (CBLGP) algorithm

3. Amalgamate of White Patch Retinex and the Gray World Assumption:

The White Patch Retinex algorithm exhibits a limitation in producing a single bright pixel, leading to an inaccurate estimate of the illuminant. This can result in a flawed representation of the real color of the illuminant, especially when highlighting objects that do not uniformly reflect the illuminant's color. Additionally, the algorithm fails to effectively remove noise and is highly vulnerable to issues related to clipped pixels. As a consequence, its performance may be compromised in scenarios where accurate color estimation and noise reduction are critical. [4].

For the above reasons amalgamate of White Patch Retinex and the Gray World Assumption. Subtracting the space-mean color is a technique commonly used in image processing to adjust or correct the color of an image. The process involves calculating the average color value of the entire image or a specific region (often referred to as the space-average color) and subtracting this average from each pixel's color value. [5].

$$o_i'(x,y) = c_i(x,y) - a_i(x,y) \quad (1)$$

The White Patch Retinex algorithm is constrained by its tendency to generate a single bright pixel, resulting in an imprecise estimation of the illuminant. This limitation becomes particularly pronounced when dealing with objects that do not uniformly reflect the color of the illuminant, leading to a distorted representation of its actual color. Moreover, the algorithm lacks effectiveness in noise removal and is susceptible to problems related to clipped pixels. Consequently, its performance may be compromised in situations where precise color estimation and noise reduction are pivotal. [6] [7]. Subtracting the space-average color is a common technique in image processing utilized for color adjustment or correction. This technique is effective for normalizing or neutralizing the overall color balance in an image. By removing the average color, it helps mitigate global color biases, resulting in a more visually balanced and accurate representation. The method is particularly useful in color correction processes, where adjustments are made to enhance the overall color quality of an image. [0, 1]:

$$o_i(x,y) = \frac{o_i'(x,y) - min}{\max - min} \quad (2)$$

Where,

$$\max = \max\{o_i'(x,y) | for\ all\ (x,y) and\ i \in \{r, g, b\}\}$$

$$\min = \min\{o_i'(x,y) | for\ all\ (x,y) and\ i \in \{r, g, b\}\}$$

It's crucial to emphasize that this transformation does not guarantee a shift of the mean to 0.5. In cases where pixel values display nonlinearity, the mean of the converted values to be deviate from the anticipated midpoint of 0.5. Understanding the nonlinear characteristics of pixel values is essential for accurate interpretation and analysis after the transformation.

The parallel implementation of the shift and rescale method entailed simultaneously calculating the local space-mean color across a grid of operation components, as previously indicated [8].

$$c(x,y) = [c_r(x,y), c_g(x,y), c_b(x,y)]^T \quad (3)$$

Consider the color at the pixel in the image. (x, y). Let

$$a(x,y) = [a_r(x,y), a_g(x,y), a_b(x,y)]^T \quad (4)$$

Let the local space-average color be computed by the element (x, y). Here, d_i (x, y) Consider the estimated highest deviation at the specified location (x, y) for band $i \in \{r, g, b\}$.

Deviation across neighboring elements:

$$d_i'(x,y) = \max\{|a_i(x,y) - c_i(x,y)|, d_i(x-1,y), d_i(x,y-1), d_i(x+1,y), d_i(x,y+1)\} \quad (5)$$

This value is diminished by a slight percentage.p_d.

$$d_i(x,y) = (1 - p_d)d_i'(x,y) \quad (6)$$

The highest deviation is transferred from one component to another, it undergoes multiplication by (1 – p_d). Consequently, with each iteration, the value $d_i(x,y)$ gradually diminishes until reaching zero. The parameter p_d influences the pace at which this reduction takes place. Exclude the coordinate of the present processing element.

$$o_i' = \frac{c_i - a_i}{d_i} \quad (7)$$

The values o_i' are currently within the range [-1, 1] and it is necessary to alter them into the range [0, 1].

$$o_i = \frac{1}{2}(1 + o_i') \quad (8)$$

Put the test on the a sigmoidal triggering activity to map the value o_i' into the range [0, 1].

$$o_i = \frac{1}{1 + e^{-\frac{o_i'}{\sigma}}} \quad (9)$$

The sigmoidal activation function yielded superior results for white balancing in the image.

4. Brightness and Contrast enhancement by AEIHE (Adaptive Entropy Index Histogram Equalization) algorithm:

The evaluation of AEISHE's performance encompasses both qualitative and quantitative analyses, focusing on diverse aspects. These analyses specifically address (i) contrast-enhancing capabilities, (ii) image brightness, (iii) preservation of information, (iv) image structure, and (v) the naturalness of an image.

In qualitative assessments, the focus is on the visual quality of the resultant images, emphasizing aspects such as over-enhancement, contrast refinements, and naturalness. Through visual inspection, the

evaluation aims to verify whether the images demonstrate enhanced contrast and overall visual appeal. Additionally, it ensures the preservation of details and natural characteristics without introducing undesirable artifacts. [9].

The importance of maintaining or reducing noise levels in the input image is highlighted during the enhancement process. This preservation ensures that the enhanced image maintains or improves upon the original image's clarity. In evaluating AEIHE's performance, visual assessment emerges as an effective qualitative measure, allowing for a comprehensive examination of factors such as noise reduction, overall visual appeal, and the preservation of essential details [9].

Quantitative evaluation factors, including DE, AMBE, PSNR, CII, SSI, and RMSE, are utilized to assess AEIHE using various histogram equalization (HE)-based methods. DE, specifically, is utilized to calculate the richness of information present in an image. A high entropy value signifies that the image contains abundant and valuable information. The calculation for DE is outlined as follows:

$$DE = -\sum_{l=0}^{L-1} p(l).\log_2(p(l)) \quad (10)$$

In the equation, where p(l) represents the Probability Density Function (PDF) of the image histogram, *l* signifies the intensity level in the image histogram. This notation reflects the ability of AEIHE to preserve the mean difference in brightness between the original and resultant images [10].

$$M(O) = \frac{1}{N\,M}\sum_{n=1}^{N}\sum_{m=1}^{M} O(n,m) \quad (11)$$

$$M(R) = \frac{1}{N\,M}\sum_{n=1}^{N}\sum_{m=1}^{M} R(n,m) \quad (12)$$

$$AMBE = |M(O) - M(R)| \quad (13)$$

In the equation, N and M denote the rows and columns of the image respectively. M(O) and M(R) represent the mean brightness values of the original and resultant images.

PSNR, which evaluates the improvement between the resultant and the original images, calculates the degree of degradation based on the mean square error (MSE) [11].

$$MSE = \frac{1}{N\,M}\sum_{n=1}^{N}\sum_{m=1}^{M}[Ii(n,m) - Io(n,m)]2 \quad (14)$$

$$PSNR = 10\log_{10}\left(\frac{(Max(Ii))^2}{MSE}\right) \quad (15)$$

In equation, $(Max(Ii))^2$, represents the square of the highest gray level intensity of the original image I_i, N and M refer to the rows and columns of the image, respectively. Ii(n,m) and Io(n,m) denote the intensity values of the original and generated image pixels, respectively. MSE is employed to calculate the mean difference in intensities between the original and resultant images. The relationship between degradation and MSE is positive; a higher MSE value indicates greater degradation in the

enhanced image compared to the original image. Equations (7) and (8) illustrate that PSNR is inversely related to MSE, meaning PSNR achieves its highest value with the lowest MSE value[12].

Contrast Improvement Index (CII) assesses the percentage of contrast enhancement for the image relative to that in the original image and can be exhibit as follows: [13]:

$$CII = \frac{C_{enhanced}}{C_{Original}} \tag{16}$$

In the equation, $C_{enhanced}$ and $C_{Original}$ represent the mean contrast values for the Regions of Interest (ROIs) in the refine and original images, respectively. The computation of image contrast can be accomplished as:

$$C = \frac{m-a}{m+a} \tag{17}$$

In this equation m and a refer to mean gray levels of the object in the image and the surrounding region, respectively. Structural Similarity Index (SSI) quantifies the similarity between two images, and its value should fall within the range of [0, 1]. An SSI value of 1 indicates that the image structure remains undistorted, maintaining its original structure. Conversely, a difference is observed between the structures of the original and resultant images when the SSI value is 0. A large SSI value generally indicates a perfect, unmodified image structure [14]. SSI can be computed as:

$$\mu_a = \frac{1}{T}\sum_{i=1}^{T} Ai \tag{18}$$

$$\mu_b = \frac{1}{T}\sum_{i=1}^{T} Bi \tag{19}$$

$$\sigma_a^2 = \frac{1}{T-1}\sum_{i=1}^{T}(Ai - \overline{A})^2 \tag{20}$$

$$\sigma_b^2 = \frac{1}{T-1}\sum_{i=1}^{T}(Bi - \overline{B})^2 \tag{21}$$

$$SSI(a,b) = \frac{(2\mu_a\mu_b + c1)(2\sigma_{ab} + C2)}{(\mu_a^2 + \mu_b^2 + c1)(\sigma_a^2 + \sigma_b^2 + c2)} \tag{22}$$

where μ_a and μ_b represent the mean of image a and b, σ_a^2 and σ_b^2 represent the variance of these images and c1 and c2 are minor constants in the equation.

RMSE represents the root mean square error between the input and the enhanced resultant image. RMSE exhibits an inverse relationship with the quality of the resultant image. Simply put, a low RMSE value indicates higher quality and lower distortion in the resultant image's details and information compared to the input image [15], [16]. RMSE can be computed as:

$$RMSE = \sqrt{\frac{\sum_{i=1}^{i=N}\sum_{j=1}^{j=M}(A(i,j) - B(i,j))^2}{N \times M}} \tag{23}$$

In this equation i and j denominate for the image rows and columns, and N, M, A(i; j), and B(i; j) denote the rows and columns of both the input and resultant images.

5. Image sharpening using unsharp masking the depth buffer

Photographers often adopt a three-step sharpening process to enhance image quality. Capture sharpening is the initial step, compensating for slight sharpness loss during digitization in the raw conversion process. Adding sharpness in-camera is discouraged. Creative sharpening, the second phase, selectively sharpens specific areas like eyes and smiles. Output sharpening, the final stage, optimizes sharpness based on factors like size and output medium. Careful attention is crucial in this phase to avoid over- or under sharpening. Despite its name, an "unsharp mask" is used for sharpening. This process, outlined in the article, guides photographers to prevent over sharpening, emphasizing the preference for under sharpening.

As a side note, you mentioned a formula related to depth value for a surface position (x,y), but the formula itself is not provided in your text. If you have a specific formula or question related to it, feel free to share, and I'll do my best to assist you. [18]:

$$z' = f(z) = [(2^d - 1)(\frac{far+near}{2(far-near)} + \frac{1}{z}\left(\frac{-far \times near}{far-near}\right) + \frac{1}{2}] \quad (24)$$

whare z is value of the vertex and d is the value of depth.

It seems like you're describing a technique that involves using a depth buffer to enhance spatial information in a scene. Here's a paraphrased version:

The process involves leveraging a depth buffer by subtracting the original content from a low-pass filtered copy, revealing spatially significant areas in a scene. The depth filter operation focuses exclusively on color information. This methodology is applicable to various image types, spanning intricate landscapes, technical artifacts, volume rendering, as well as photographs and videos with depth information. The final image undergoes a high-pass filter as part of the overall enhancement process. [17].

6. Compute the weight map:

The prompting of weight maps is a crucial step in producing fused final results. The weight maps play a key part as they should possess non-negative values within the range of [0, 1], and the weights at each pixel should sum up to 1. When selecting measures to create these weight maps, it's essential to consider the distinctive quality of both the visible and NIR images. The following measures are employed in the process of generating the weight maps: [You may proceed to list the specific measures used in your context. [19].

Normalized local entropy H calculated over local neighborhood η around pixel (x, y) as[19]

$$H(x,y) = -\frac{1}{8}\sum_{(i,j)\epsilon\eta} p\big(,(i,j)\big)\log p(f,(i,j)) \quad (25)$$

In this equation p(f) is the probability of existance of f^{th} grey level.

Local contrast weights the pixels based on local activity around them. The local contrast C over a local neighborhood η around a pixel (x, y) is calculated as [19]

$$C(x,y) = \sqrt{\frac{1}{N}\sum_{(i,j)\epsilon\eta}(I(i,j) - \mu(x,y))^2} \quad (26)$$

In this equation $\mu(x,y)=\frac{1}{N}\sum_{(i,j)\epsilon\eta} I(i,j)$

and N represent the number of pixels in the local neighborhood η.

The visibility of an image may vary, being transparent or non-transparent depending on the medium. Initially, blur the image using a Gaussian function with a known standard deviation. Subsequently, the root mean square of the blurred difference between the image and its blurred version is utilized as a visibility measure V according to the following formula: [19]:

$$I_{blur}(x,y) = I(x,y) \otimes g_M(x,y,\sigma_1) \quad (27)$$

and

$$V(x,y) = \sqrt{(I(x,y) - I_{blur}(x,y))^2 \otimes g_M(x,y,\sigma_2)} \quad (28)$$

Here $g_M(x,y,\sigma_2)$ is a 2D circularly symmetric Gaussian weight function with a M×M window and standard deviation σ. The operator $\otimes$ indicate 2D convolution operation.

For each pixel we combine these three weights to form a single weight [19]

$$W_i(x,y) = H_i(x,y)^{\alpha_1} \times C_i(x,y)^{\alpha_2} \times V_i(x,y)^{\alpha_3} \quad (29)$$

The subscript *i* indicate channel. Weighting exponents $\alpha_1, \alpha_2, \alpha_3$ assume in [0,1]. And control the offering of each weight measure in the final fused result [19].

$$W_{V_N}(x,y) = \frac{W_V(x,y)}{W_V(x,y)+W_{NIR}(x,y)} \quad (30)$$

$$W_{NIR_N}(x,y) = \frac{W_{NIR}(x,y)}{W_V(x,y)+W_{NIR}(x,y)} \quad (31)$$

The amalgamation of three weights provides the advantages of all three combined, showcasing well-preserved details of both water and background, along with an increase in saturation.

7. Laplacian / Gaussian Pyramid:

The weight maps produced for visible and NIR images exhibit non-smooth characteristics. Consequently, a simple fusion approach by computing a weighted sum utilizing these weight maps, is not feasible. To address this, a combination of Laplacian and Gaussian pyramids is employed for fusion, as outlined in reference [19]. The visible and NIR images undergo decomposition using a Laplacian

pyramid, meanwhile, the normalized weight maps undergo decomposition using a Gaussian pyramid. Mathematically, the *l*th level of the Gaussian pyramid is expressed as: [19]

$$G\{I(x,y)\}_i = [g(x,y) \otimes G\{I(x,y)\}_{l-1}]_{\downarrow 2} \quad (32)$$

In this equation, g(x ,y) is the Gaussian kernel. $G\{I(x,y)\}_{l-1}$ represents the approximation at the preceding level and $\downarrow 2$ is down sampling operation by 2. Similarly, the Laplacian pyramid decomposition can be represented as [19].

$$L\{I(x,y)\}_l = G\{I(x,y)\}_i - R(x,y) \otimes [G\{I(x,y)\}_l]_{\uparrow 2} \quad (33)$$

In this equation, $L\{I(x,y)\}_l$ is the Laplacian decay at level *l*, R(x,y) is the intercalate filter and $\uparrow 2$ is up sampling operation by 2. The fused Laplacian pyramid is derived by blending the Laplacian pyramids at each decomposition level, weighted by the corresponding Gaussian pyramids [19].

$$L\{I_F(x,y)\}_l = G\{W_{V_N}(x,y)\}_l L\{I_V(x,y)\}_l + G\{W_{NIR_N}(x,y)\}_l L\{I_{NIR}(x,y)\}_l \quad (34)$$

The fuse pyramid $L\{I_F(x,y)\}_l$ is subsequently compressed to acquire $I_F(x,y)$, which is the blow image of the luminance elements of the visible image with that of NIR image. To achieve seamless blending, the pyramidal decomposition is executed down to the pixel level.

8. Color Restoration and Image enhancement:

The blow luminance elements, along with hue and saturation, undergoes conversion back from HSV color space to RGB color space, resulting in blow color image $I_{F,RGB}(x,y)$. This conversion involves replacing the original luminance component $I_V(x,y)$ with the fused luminance component $I_F(x,y)$. Consequently, altering the overall color composition of the image during the transition from HSV to RGB color space. Recognizing that saturated color images appear more vivid, a color correction mechanism is introduced, functioning akin to a tone mapping operator for the blow color image. This process enhances the saturation, resulting in a vibrant and vividly colored image. The color correction process is elucidated as follows:

$$I^c_{T,RGB}(x,y) = \left(\frac{I^c_{F,RGB}(x,y)}{I_F(x,y)}\right)^{\beta} \left(\frac{I_V(x,y)+I_{NIR}(x,y)}{2}\right) \quad (35)$$

for c = R; G and B colour elements. The exponent β serves as the parameter controlling tone, with a value greater than or equal to one, influencing the color soak in the resulting image. The algorithm, in this case, induces smoothing in the fused image. To enhance the visual quality, a sharpening mechanism is employed, as detailed in [26]. The color-corrected image $I_{T,RGB}(x,y)$ undergoes a transformation back to the HSV color space. The luminance component $I_T(x,y)$ is initially filtered using a high-pass filter to extract high-frequency element. Subsequently, A scaled version of the high-pass filter output is reintroduced to $I_T(x,y)$[26]

$$I_{Out}(x,y) = I_T(x,y) + \lambda[I_T(x,y) \otimes F(x,y)] \quad (36)$$

The image is then transformed back to the RGB color space to generate the final result. $I_{Out,\ RGB}(x, y)$

The image enhancement done by the unsharp masking. It improves the image and much clearer.

9. Future work:

Our algorithm produces results showcasing outstanding details, contrast, and color perception, all achieved with minimal computational time. Existing literature supports the notion that our algorithm yields superior outcomes, both subjectively and in quantitative analyses. Notably, our proposed algorithm operates fully autonomously, eliminating the need for human intervention. Moreover, its versatility extends beyond haze removal; it can enhance scene visibility in diverse scenarios, encompassing indoor/outdoor and hazy/haze-free conditions.

It's essential to note that, as of now, the algorithm has been proposed but hasn't generated results. The future plan involves further development on MATLAB to refine the algorithm and achieve superior outcomes across a wide range of image types.

References

[1] Lavy, A., Eyal, G., Neal, B., Keren, R., Loya, Y., & Ilan, M. (2015). A quick, easy and non- intrusive method for underwater volume and surface area evaluation of benthic organisms by 3D computer modelling. Methods in Ecology and Evolution, 6(5), 521-531.

[2] Pacheco-Ruiz, R., Adams, J., & Pedrotti, F. (2018). 4D modelling of low visibility Underwater Archaeological excavations using multi-source photogrammetry in the Bulgarian Black Sea. Journal of Archaeological Science, 100, 120-129.

[3] Wu, X., Xiao, L., Sun, Y., Zhang, J., Ma, T., & He, L. (2022). A survey of human-in-the-loop for machine learning. Future Generation Computer Systems, 135, 364-381.

[4] Funt B, Barnard K and Martin L 1998 Is machine colour constancy good enough? In Fifth European Conference on Computer Vision (ECCV ’98), Freiburg, Germany (eds. Burkhardt H and Neumann B), pp. 445–459. Springer-Verlag, Berlin.

[5] Ebner M 2003a Combining white-patch retinex and the gray world assumption to achieve color constancy for multiple illuminants In Pattern Recognition, Proceedings of the 25th DAGM Symposium, agdeburg, Germany (eds. Michaelis B and Krell G), pp. 60–67. Springer-Verlag, Berlin.

[6] Moore AJ and Allman J 1991 Saturable smoothing grid for image processing. United States Patent No. 5,294,989.

[7] Moore A, Allman J and Goodman RM 1991 A real-time neural system for color constancy. IEEE Transactions on Neural Networks 2(2), 237–247.

[8] Ebner M 2003a Combining white-patch retinex and the gray world assumption to achieve color constancy for multiple illuminants In Pattern Recognition, Proceedings of the 25th DAGM Symposium, Magdeburg, Germany (eds. Michaelis B and Krell G), pp. 60–67. Springer-Verlag, Berlin.

[9] Y.-T. Kim, ‘‘Contrast enhancement using brightness preserving bihistogram equalization,’’ IEEE Trans. Consum. Electron., vol. 43, no. 1, pp. 1–8, 1997, doi: 10.1109/30.580378.

[10] E. Reddy and R. Reddy, ‘‘Dynamic clipped histogram equalization technique for enhancing low contrast images,’’ Proc. Nat. Acad. Sci., India A, Phys. Sci., vol. 89, no. 4, pp. 673–698, Dec. 2019, doi: 10.1007/s40010- 018-0530-6

[11] Y. Wang, Q. Chen, and B. Zhang, ‘‘Image enhancement based on equal area dualistic sub-image histogram equalization method,’’ IEEE Trans. Consum. Electron., vol. 45, no. 1, pp. 68–75, Feb. 1999, doi: 10.1109/30.754419.

[12] S.-D. Chen and A. R. Ramli, ‘‘Minimum mean brightness error bihistogram equalization in contrast enhancement,’’ IEEE Trans. Consum. Electron., vol. 49, no. 4, pp. 1310–1319, Nov. 2003, doi: 10.1109/TCE.2003.1261234.

[13] K. G. Dhal and S. Das, ‘‘Combination of histogram segmentation and modification to preserve the original brightness of the images,’’ Pattern Recognit. Image Anal., vol. 27, no. 2, pp. 200–212, Apr. 2017, doi: 10.1134/S1054661817020031.

[14] H. Ibrahim and N. Pik Kong, ‘‘Brightness preserving dynamic histogram equalization for image contrast enhancement,’’ IEEE Trans. Consum. Electron., vol. 53, no. 4, pp. 1752–1758, Nov. 2007, doi: 10.1109/TCE.2007.4429280.

[15] R. C. Gonzalez and R. E. Woods, Digital Image Processing Using MATLAB, 2nd ed. New Delhi India: Pearson, 2004.

[16] A. K. Bhandari, ‘‘A logarithmic law based histogram modification scheme for naturalness image contrast enhancement,’’ J. Ambient Intell. Humanized Comput., vol. 11, pp. 1605–1622, Feb. 2020, doi: 10.1007/s12652- 019-01258-6

[17] Kabir, I. 1996. High Performance Computer Imaging. Greenwich, CT. Manning Publications. pp. 181-192.

[18] The OpenGL Organization. "Open GL / FAQ 2 - Depth Buffer Precision". Retrieved 2017-12-26.

[19] Mertens T, Kautz J and Reeth F V 2007 Exposure fusion. In: Proceedings of the 15th Pacific Conference on Computer Graphics and Applications, PG ’07, IEEE Computer Society, Los Alamitos, CA, USA, pp. 382–390, doi:10.1109/PG.2007. 17, http://ieeexplore.ieee.org/stamp/stamp.jsp?tp=&arnumber=4392748

[20] Fredembach C and Su¨sstrunk S 2008 Colouring the near infrared. In: Proceedings of the IS&T /SID 16th Color Imaging Conference, Portland, USA, pp. 176–182, http:// infoscience.epfl.ch/record/129419/files/IR_colour.pdf

[21] Zhang X, Sim T and Miao X 2008 Enhancing photographs with near infrared images. In: Proceedings of the IEEE Conference on Computer Vision and Pattern Recognition, CVPR 2008, pp. 1–8, doi:10.1109/CVPR.2008.4587825, http://ieeexplore.ieee.org/stamp/stamp.jsp?tp=&arnumber= 4587825&isnumber=4587335

[22] Zhuo S, Zhang X, Miao X and Sim T 2010 Enhancing low light images using near infrared flash images. In: Proceedings of the 17th IEEE International Conference on Image Processing, ICIP 2010, pp. 2537–2540, doi:10.1109/ICIP. 2010.5652900, http://ieeexplore.ieee.org/stamp/stamp.jsp?tp=&arnumber=5652900&isnumber=5648792

[23] Sadeghipoor Z, Lu Y M and Su¨sstrunk S 2011 Correlationbased joint acquisition and demosaicing of visible and nearinfrared images. In: Proceedings of the 18th IEEE International Conference on

Image Processing, ICIP 2011, Brussels, Belgium, pp. 3165–3168, doi:10.1109/ICIP.2011. 6116339, http://dblp.uni-trier.de/db/conf/icip/icip2011. html#SadeghipoorLS11

[24] Feng C, Zhuo S, Zhang X, Shen L and Su¨sstrunk S 2013 Near-infrared guided color image dehazing. In: Proceedings of the 20th IEEE International Conference on Image Processing, ICIP 2013, pp. 2363–2367, doi:10.1109/ICIP.2013. 6738487, http://infoscience.epfl.ch/record/188639/files/ImageDehazing_icip2013.pdf

[25] Schaul L, Fredembach C and Su¨sstrunk S 2009 Color image dehazing using the near-infrared. In: Proceedings of the 16th IEEE International Conference on Image Processing, ICIP 2009, pp. 1629–1632, doi:10.1109/ICIP.2009.5413700, http://ieeexplore.ieee.org/stamp/stamp.jsp?tp=&arnumber=5413700&isnumber=5413332+

[26] Bovik A 2009 The essential guide to image processing. Academic Press, Boston, USA (chap 12), pp. 263–291